
Article:
Liamas, E orcid.org/0000-0001-9294-6343, Thomas, ORT, Muñoz, AI et al. (1 more author) (2020) Tribocorrosion behaviour of pure titanium in bovine serum albumin solution: A multiscale study. Journal of the Mechanical Behavior of Biomedical Materials, 102. 103511. ISSN 1751-6161

https://doi.org/10.1016/j.jmbbm.2019.103511

Tribocorrosion behaviour of pure titanium in bovine serum albumin solution: a multiscale study

Evangelos Liamas,[1] Owen R.T. Thomas,[1] Anna Igual Muñoz,[2,3,#] and Zhenyu J. Zhang[1,*]

[1]School Chemical Engineering, University of Birmingham, Edgbaston, Birmingham B15 2TT U.K.

[2]Department of Chemical and Nuclear Engineering, Universidad Politécnica de Valencia, Valencia, E-46071, Spain

[3]School of Engineering, Materials Science and Engineering, EPFL, MXC 341 (Bâtiment MXC), Station 12, CH-1015, Lausanne, Switzerland

To whom correspondence should be addressed.

[#]Email: anna.igualmunoz@epfl.ch

[*]Email: z.j.zhang@bham.ac.uk

Abstract

Tribocorrosion behaviour of pure titanium in phosphate buffer saline (PBS) solution has been investigated systematically as a function of surface chemistry and bovine serum albumin (BSA) content in the solution. A ball-on-disk tribometer coupled with an electrochemical cell was used to study the effect of electrochemical conditions (i.e. anodic and cathodic applied potentials, as well as at open circuit potential) on the tribocorrosion response of titanium. It was found that the main material loss is due to mechanical wear caused by plastic deformation. The mechanical wear was higher under anodic conditions than under cathodic, partially due to an increased presence of debris particles at the sliding interface that act as third bodies. The effect of BSA on the interaction between alumina and titanium, as well as the behaviour of third bodies during the mechanical wear, were investigated in the nanoscale level using atomic force microscopy based force spectroscopy. It was found that the presence of BSA affects tribocorrosion in various ways. Firstly, it increases the repassivation rate of the oxide film by inhibiting the cathodic reactions and accelerating the anodic reactions. Secondly, it increases the mechanical wear by increasing the adhesion of debris onto the sliding interface, while at anodic conditions it increases the rolling efficiency of the debris particles that further enhances the mechanical wear.

Keywords: BSA, AFM, Force spectroscopy, Protein adsorption

1 Introduction

Due to a combination of outstanding mechanical properties and high biocompatibility, titanium and titanium alloys are widely used materials in biomedical applications. Among others, they exhibit a high strength to weight ratio, a modulus of elasticity similar to bone that makes the bone-to-implant interface closely matched, and an exceptional resistance to corrosion.[1, 2, 3, 4] Similar to most other metallic biomaterials, the corrosion resistance of titanium is highly depended on a thin and inert oxide film present on its surface, which is developed when the metal is exposed to ambient or liquid environments. Such passive oxide layer contributes substantially towards the exceptional biocompatibility of titanium - it protects the underlying substrate from corrosion when being placed in physiological environment, and provides an excellent interface to interact with the surrounding tissue that can prevent inflammatory responses.[5] Furthermore, the oxide layer acts as a barrier to restrict release of ions that could react with biomolecules and cause cytotoxicity, allergies, or other biological influences.[6] The titanium oxide has an isoelectric point of 5-6 which results in a slightly negatively charged surface in physiological pH.[7] The aforementioned characteristics enable titanium and its alloys being used in a wide range of biomaterials, from dental implants to hip joints.[7, 8, 9, 10] However, the performance of titanium is degraded when it is subjected to a tribological contact in a corrosive environment, due to its poor tribocorrosion resistance.[11]

A tribocorrosion system combines corrosion and mechanical wear as mechanisms of degradation. The two mechanisms cannot be considered separately but rather as a complex system where one is dependent on the other; corrosion is accelerated by wear, and analogously, wear can be affected by corrosion.[12] Upon sliding, the oxide layer that covers the titanium surface is removed (depassivation), leaving the active titanium exposed to the aggressive physiological

environment. As a result, the corrosion rate is increased (wear accelerated corrosion). The passive film is then progressively reformed on the surface (repassivation) and protects the substrate from further corrosion. Furthermore, the presence of a passive film (i.e. electrochemical conditions) can also influence the mechanical response of titanium in a tribocorrosion system.[13]

The effect of the passive film on tribocorrosion process can be determined by the nature of the material, the prevailing electrochemical and mechanical conditions, and the surrounding environment. Various combinations of the aforementioned factors create a distinct tribocorrosion system that affects differently the passive film of the metals and, thus, their corrosion process. For instance, studies on hafnium and pure titanium in sodium chloride (NaCl) solution showed that the passive film formed on their surface acts as a barrier to protect against corrosion, as expected, while mechanical damage disrupts the passive film that is quickly reformed when the damage is ceased.[14] However, hafnium shows a faster repassivation rate than pure titanium, highlighting the different anti-corrosion behaviour due to the nature of materials. The presence and thickness of the passive film, which is highly depended on the prevailing electrochemical conditions, not only affects the corrosion behaviour of a metal but also its mechanical behaviour. For instance, the absence of a passive film on carbon steel (DIN 34CrNiMo6) in borate solution could reduce the rate of mechanical wear because the detached metallic particles are readily smeared back on the wear track under the applied pressure.[15] In contrast, the presence of a passive film in the same system results in detachment of the passive film from the surface of the steel, and the consequent wear-accelerated corrosion. Similar results with that of carbon steel were reported for CoCrMo implants, while it was further observed that the surface degradation is influenced by the prevailing electrochemical conditions.[13] It was shown that not only the corrosion is greater in the area where

82 the metals rubbing with each other due to wear-accelerated corrosion, but also the area surrounding
83 the contact site have increased corrosion due to galvanic coupling between the worn area and the
84 surrounding passive metal.
85
86 Chemical composition of the electrolyte has been shown to have a significant impact on the
87 tribocorrosion resistance of metal and alloys. Various ions and proteins present in the liquid,
88 particularly in physiological environment, can affect the characteristics of the passive film.[16]
89 However, the reported effects of proteins on the behaviour of passive film are inconsistent and
90 highly dependent on the nature of the metal and the type of protein used. For instance, on titanium
91 alloys under fretting conditions, albumin did not affect neither the wear rate nor the wear-
92 accelerated corrosion, while collagen slightly reduced the wear rate at the cathodic potential.[17]
93 Similar results were reported with a series of titanium alloys – the presence of protein can either
94 reduce or increase the degradation of the material, depending on the alloy and the type of wear.[18]
95 It was also suggested that the presence of BSA on pure titanium could accelerate the repassivation,
96 which is caused by the adsorbed proteins that act as a barrier and prevent the water from reaching
97 the titanium surface.[19] However, when abrasive particles are involved, the presence of BSA leads
98 to accelerated wear, which is attributed to an enhanced particle entrainment and a greater rolling
99 efficiency of the particles.[20]
100
101 Although there have been several studies investigating various tribocorrosion systems, an in-
102 depth understanding on the tribocorrosion characteristics of pure titanium in PBS and albumin
103 solution, under cathodic and anodic applied potential, is missing. The aim of the present study is
104 to examine the aforementioned characteristics on the micro- and nanoscale. A pin-on-disk

tribometer, coupled with an electrochemical cell, was utilized in order to perform tribocorrosion experiments of pure titanium in PBS and albumin solutions. The experiments were performed both under cathodic and anodic polarization conditions to understand the effect of the prevailing electrochemical conditions on the wear of the titanium surface. Furthermore, atomic force microscopy was employed to measure the interactions between the studied surfaces at the nanoscale and how they are affected by the presence of albumin.

2 Materials and methods

2.1 Materials

Pure titanium substrates (99.99+% purity, Cat. no. 754-091-17) were purchased from Goodfellow Cambridge Ltd (754-091-17, Huntingdon, UK). Polished AT-cut, 5 MHz, 1-inch diameter titanium coated quartz crystals (Cat. no. 750-1029-G1, purity 99.995%) were purchased from Testbourne Ltd (Basingstoke, UK), and used for nanoadhesion measurements. Alumina particles (Cat. no. 46025) were purchased from Alfa Aesar (Lancashire, UK). Atomic force microscope (AFM) cantilevers (Cat. no. PNP-TR-TL) were purchased from NanoWorld AG (Neuchatel, Switzerland). Fatty acid free (> 99%, Cat. no. A0281) bovine serum albumin (BSA) was purchased from Sigma-Aldrich Company Ltd (Dorset, UK), while phosphate buffer saline (PBS) (Cat. no. P3203-100) and sodium dodecyl sulphate (SDS) (Cat. no. 10090490) were purchased from Fisher Scientific (Loughborough, UK).

2.2 Sample preparation

The bulk titanium sample was cut to 25 mm by 25 mm squares. Before each experiment, the sample was wet-ground with 500 to 4000 grit SiC paper and further polished with OP-Chem polishing cloths using 1 µm diamond particles to achieve a mirror-like finishing. Following the

129 polishing treatment, the samples were ultrasonically cleaned in sodium dodecyl sulphate solution
130 followed by distilled water for 10 min respectively, which ensured the removal of any particles or
131 protein from the surface. Lastly, the surfaces were dried in a stream of compressed air. The
132 cleaning procedure for the QCM crystals was the same as with the bulk titanium. BSA solutions
133 were prepared using the PBS buffer to obtain protein concentration of 1 mg/mL.
134

135 **2.3 Tribocorrosion tests**

136 All electrochemical measurements were carried out using a Solartron Analytical 1286
137 potentiostat by Ametek (Berwyn, Pennsylvania, USA). The set-up is a three-electrode
138 electrochemical cell, using a platinum wire as counter electrode and an Ag/AgCl (3M KCl)
139 reference electrode. All potentials were referred to the reference electrode (0.205 V versus standard
140 hydrogen electrode, SHE).
141

142 For the tribocorrosion tests, a unidirectional pin-on-disk rotating tribometer coupled to a
143 potentiostat was used. The titanium specimen was mounted on the tribometer with its lower part
144 insulated and electrically connected to the working electrode of the potentiostat, while its upper
145 surface (2.06 cm^2) was exposed to the electrolyte solution. The reference electrode was kept within
146 1 cm away from the titanium surface. An alumina sphere with a diameter of 6 mm was used as a
147 counterpart.[21] A normal force of 5 N was applied on the counterpart, corresponding to a maximum
148 contact pressure of approximately 950 MPa using the Hertzian contact stress model[22] (Poisson's
149 ratio equal to 0.23 and 0.34, and Young's modulus equal to 380 and 103 GPa, for alumina and
150 pure titanium respectively). The sliding velocity and duration were set to 60 rpm (equivalent to
151 1.13 m/min) and 30 min respectively, and the radius of the wear track was set at 3 mm. The tests
152 were performed both in 1xPBS and protein solution (1 mg/mL) at 3 different surface potential

153 conditions. Including open circuit potential (OCP), -1.2 $V_{Ag/AgCl}$, and +1.0 $V_{Ag/AgCl}$. The applied
154 potentials were selected to match the cathodic and the anodic areas of the titanium, as studied
155 systematically in a separate work.[24] All measurements were repeated 3 times to ensure the
156 reproducibility.
157
158 An Olympus LEXT OLS3000 confocal microscope (Tokyo, Japan) was used to carry out the
159 post examination of the wear track, including both surface morphology and the quantification of
160 wear volume. A JEOL JSM-6300 scanning electron microscope (Westmont, Illinois, USA) was
161 used to image and analyse the wear tracks on the titanium surface and the alumina counterpart. A
162 G200 Nanoindenter by Keysight Technologies UK Limited (Berkshire, UK) was used to determine
163 the microhardness of the material both inside and outside the wear track by employing a diamond
164 tip to apply a pressure of 0.2 kgf/mm^2 (1.96 MPa) for a duration of 15 s (Hv0.2/15).
165
166 **2.3 Force spectroscopy**
167 Individual alumina particles were attached onto tip-less AFM cantilevers using a two-part
168 epoxy glue. The colloidal cantilevers were calibrated with the thermal method[23] before the
169 attachment of the alumina particles on them (nominal spring constant is 0.08 N/m). Force
170 measurements were conducted using a Nanowizard II atomic force microscope by JPK Instruments
171 AG (Berlin, Germany) that was coupled with a PGSTAT101 potentiostat by Metrohm Autolab
172 B.V. (Utrecht, Netherlands), which is conventional three-electrode electrochemical cell, using a
173 platinum wire as counter electrode and a Dri-Ref^{TM} (3M KCl) reference electrode by World
174 Precision Instruments (Sarasota, Florida, USA). During the force spectroscopy measurements,
175 titanium-coated QCM sensors instead of titanium sheet were used as substrate. The
176 electrochemical characteristics of such titanium-coated QCM crystals were found similar to that

177 of bulk titanium.[24] The titanium coated QCM sensor crystal was mounted in the electrochemical
178 cell (working electrode) with its upper surface (1.33 cm^2) exposed to the electrolyte. The
179 experiments were conducted both in 1xPBS and in protein solution. A total of 240 force curves
180 were collected over 16 different regions of the titanium surface to ensure that the result is
181 statistically representative. Cantilever velocity was 2 μm/s with applied force being 5 nN. The
182 alumina particle was kept in contact with the surface for 0.3 s before it was retracted. All data were
183 presented as mean values ± the standard error of the mean. A statistical comparison was made
184 using a single factor analysis of variance (ANOVA) and post hoc t-stat multiple comparison testing
185 to evaluate the significance of the measured parameters.
186

187 **3 Results**

188 **3.1 Tribocorrosion tests**

189 The open circuit potential of the titanium was recorded as a function of time before, during, and
190 after sliding (Figure 1). The averaged values of OCP are shown in Table 1. Upon the initiation of
191 sliding, an abrupt reduction in OCP was observed, which is due to the mechanical removal of the
192 passive film from the surface, leaving the active titanium underneath exposed to the aqueous
193 solution. It also confirms the existence of a passive film on the titanium surface before rubbing.
194 Whilst the alumina sphere was sliding over the titanium substrate, a fluctuation on the OCP of
195 approximately 0.1 $V_{Ag/AgCl}$ was observed. It is highly likely due to the cyclic
196 depassivation/repassivation process as the result of the passive film being removed and reformed
197 continuously. The OCP during sliding was higher (in absolute value) in the protein solution than
198 that in the PBS buffer, which could be due to the presence of adsorbed BSA molecules that inhibit
199 the rate of cathodic reactions of oxygen and shift the corrosion potential towards more cathodic
200 values.[25] Once the sliding stopped, an abrupt increase in the OCP of titanium was observed, which

is slightly slower in the presence of BSA indicating a slower repassivation of titanium surface.[14] This, once again, confirms the formation of a passive film when the sliding stops.

Table 1: Averaged values and standard errors of OCP before (OCP_0), during ($OCP_{sliding}$), and after (OCP_{final}) sliding of pure titanium against an alumina sphere in 1xPBS electrolyte, with or without BSA. Data represent mean values of n=3 measurements ± standard error.

Solution	OCP_0 (mV)	$OCP_{sliding}$ (mV)	OCP_{final} (mV)
1xPBS	-388±67	-882±82	-451±77
1 mg/mL BSA	-362±26	-1018±44	-505±34

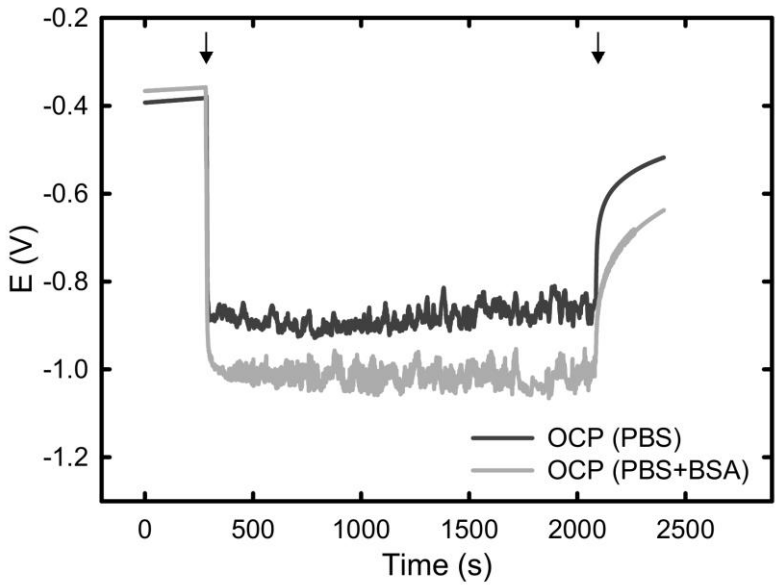

Figure 1: Evolution of the open circuit potential over time in PBS buffer with or without the presence of BSA. The graphs represent the mean values of n=3 measurements. Arrows are included in the figure to indicate where sliding starts and ends.

214 The tribocorrosion response of titanium were studied at cathodic and anodic applied potential,
215 in addition to open circuit potential. Figure 2a shows the evolution of current when a negative
216 potential of -1.2 $V_{Ag/AgCl}$ was applied to the system. Under this condition, the measured negative
217 current corresponds to the reduction reaction of the oxidant (dissolved oxygen and water) because
218 titanium oxide cannot be reduced at the selected cathodic potential.[26, 27, 28, 29, 30, 31] Indeed, this is
219 shown on the polarization curves of titanium in the studied electrolytes (Figure 3). In the cathodic
220 domain, Figure 3a, the current plateau at around -1 $V_{Ag/AgCl}$ corresponds to the mass transport
221 limited oxygen reduction. The increase (in absolute value) of the current during rubbing
222 corresponds to the increase in oxygen reduction kinetics on depassivated surfaces (arrows in Figure
223 2 indicate where sliding starts and ends). This increase in the current is significantly reduced with
224 the presence of BSA than that in PBS solution, indicating that BSA inhibits the rate of cathodic
225 reactions. A fluctuation with the current of approximately 20 μA was observed during sliding,
226 which could be due to a combined action of the dynamic equilibrium between depassivation and
227 repassivation of the surface and the increase in roughness in the wear track, thus the active area.
228 When the sliding was stopped, the current showed a steep increase due to repassivation of the
229 surface.

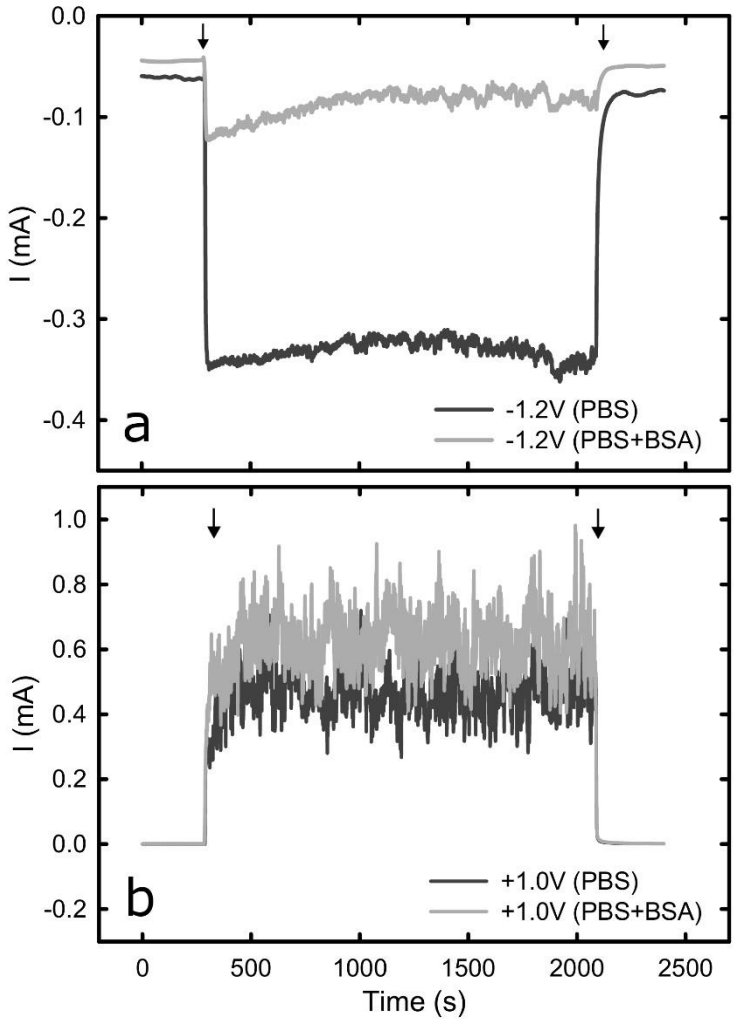

230

231 Figure 2: Evolution of the current of titanium in PBS buffer with or without the presence of BSA as a function of time
232 at (a) -1.2 $V_{Ag/AgCl}$, and (b) +1.0 $V_{Ag/AgCl}$. The graphs represent the mean values of n=3 measurements. Arrows are
233 included in the figures to indicate where sliding starts and ends.

234

235 Figure 2b shows the current evolution with time of the titanium surface when sliding against
236 the alumina counterpart at an applied passive potential (+1.0 $V_{Ag/AgCl}$) as a function of time. Before
237 the initiation of sliding, the current is approximately 0.5 µA, which indicates the presence of a
238 passive layer blocking current flow. Upon sliding, a steep increase of the current was observed,
239 suggesting the surface undergoes depassivation process (mechanical removal of passive film). The

240 current stabilizes at around 400 μA. Interestingly, the increase in current is slightly greater (~30%)
241 with the presence of BSA than that in PBS buffer, which suggests that the presence of BSA
242 accelerates the rate of anodic reactions. Indeed, the anodic polarization curve of titanium, Figure
243 3b shows a clear anodic Tafel domain around the corrosion potential with higher current densities
244 in the BSA-containing solution. When the sliding was stopped, an abrupt reduction of the current
245 was observed as a result of fast repassivation of the surface.
246

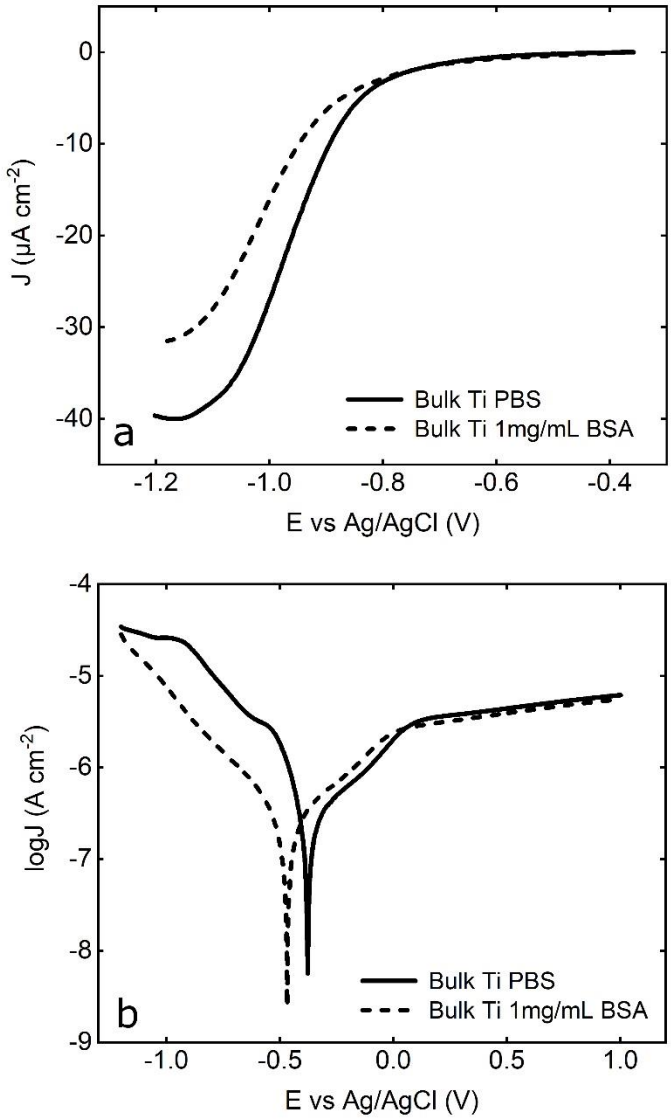

247

248 Figure 3: (a) Cathodic polarization j-E curves of bulk titanium in PBS with and without BSA, and (b) anodic
249 polarization logj-E curves of bulk titanium in PBS with or without BSA. The graphs represent the average values of
250 n=3 measurements.

251

252 The averaged values of current under each applied potential are summarized in Table 2, where
253 I_0 is the current before the initiation of sliding, $I_{sliding}$ is the average current during the sliding, and
254 I_{final} is the average current when the sliding was stopped. $I_{sliding}$ is the current that flows only
255 through the wear track and was calculated by subtracting I_0 from the overall current during sliding.
256 It was assumed that I_0 is approximately the current that flows outside the wear track since the
257 surface area was significantly larger than the area of the wear track.[32] Furthermore, the impact of
258 the presence of BSA in cathodic conditions is greater than that in anodic conditions as shown by
259 the current values when sliding starts. This suggests that the effect of BSA on the cathodic
260 reactions is significantly greater than that in anodic reactions.

261

262 Table 2: Averaged values of current before (I_0), during ($I_{sliding}$), and after (I_{final}) sliding of pure titanium against an
263 alumina sphere in 1xPBS electrolyte, with or without BSA, and in 2 different applied potentials. Data represent mean
264 values of n=3 measurements ± standard error.

$E_{applied}$ ($V_{Ag/AgCl}$)	Solution	I_0 (μA)	$I_{sliding}$ (μA)	I_{final} (μA)
-1.2 V	1xPBS	-61±9	-328±38	-75±2
	1 mg/mL BSA	-45±3	-83±24	-44±7
+1.0 V	1xPBS	0.5±0.2	470±41	0.8±0.3
	1 mg/mL BSA	0.5±0.2	629±13	1.0±0.1

265

266

267 **3.2 Wear quantification and morphology**

268 After the tribocorrosion measurements, the volume of the wear track (V_{tot}) was calculated by
269 multiplying the average cross-sectional area of the wear track by the total length of the wear track,
270 based on the acquired confocal microscopy images. Averaged wear track volumes acquired under
271 various electrochemical conditions with or without BSA are shown in Figure 4. Under OCP
272 condition, the material loss of titanium in PBS is approximately 0.18±0.02 mm^3, and is slightly
273 increased to approximately 0.22±0.02 mm^3 with the presence of protein. However, the difference
274 is insignificant ($P>0.05$) and no further conclusions can be made. The effect of applied potential
275 on the wear track volume is different at anodic and cathodic conditions. The application of cathodic
276 potential resulted in the least material loss, approximately 30% less than that at OCP. Also, the
277 presence of BSA in these conditions does not change the amount of material loss, suggesting that
278 the effect of protein is negligible at cathodic conditions. In contrast, with the application of an
279 anodic potential, the total material loss is significantly increased. In PBS it exhibits an increase of
280 approximately 60% in comparison to OCP, while the presence of protein could double the material
281 loss. To further understand the mechanisms that result is material loss, the contribution of
282 corrosion and mechanical removal was calculated.

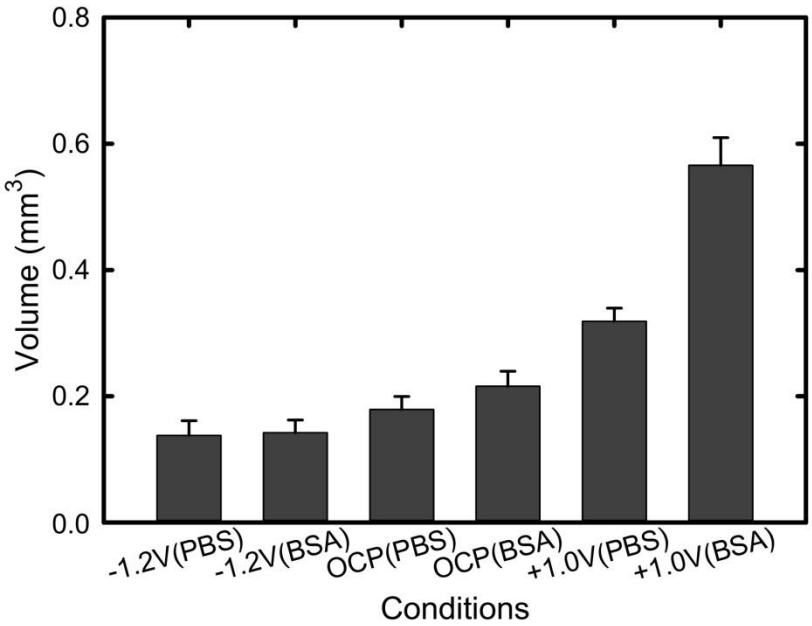

Figure 4: Wear track volume of the titanium disk under various conditions. Data points represent mean values of n=3 measurements ± standard error. The difference of protein is insignificant (P>0.05) at -1.2 V and OCP, while it is significant (P<0.05) at +1.0 V.

There are two major mechanisms that account for the overall material loss V_{tot}[33]: material removal by tribocorrosion on the sliding surface (both mechanical wear, V_{mech}, and wear-accelerated corrosion, V_{wac}) in addition to corrosion that occurs on a metallic surface when being exposed to electrolyte (V_{corr}). The latter could be considered as negligible on passive metals. Therefore, the total material loss can be expressed in Eq. 1:

$$V_{tot} = V_{mech} + V_{wac} \qquad (1)$$

The wear-accelerated corrosion is a result of the depassivation and repassivation process that occurs in the wear track during the sliding process,[27] and can be calculated using Faraday's law (Eq. 2):

$$V_{wac} = \frac{I_{sliding} \cdot t \cdot M}{n \cdot F \cdot \rho} \qquad (2)$$

where $I_{sliding}$ is the current flowing from the wear track and can be calculated by subtracting the current before sliding from the current during sliding, t is the duration of sliding (1800 s), M is the atomic mass of titanium (47.88 g mol^{-1}), n is the oxidation valence (assumed 4 for titanium[34]), F is the Faraday constant (96500 C mol^{-1}), and ρ is the density of titanium (4.51 g cm^{-3}). The contribution of mechanical wear can then be calculated by subtracting the wear-accelerated corrosion from the total material loss. Table 3 summarizes the material loss at OCP and applied potential conditions. The material loss due to wear accelerated corrosion at cathodic condition cannot be measured, while at OCP condition is negligible and hence not shown. Consequently, the total material loss at OCP and cathodic conditions is attributed to mechanical wear. For anodic conditions, approximately 7% of the total material loss is due to wear-accelerated corrosion in PBS. Although the presence of BSA increases almost by a third the wear-accelerated corrosion, the contribution in the total material loss is approximately 5%. This indicates that the presence of BSA greatly enhances the mechanical wear under anodic conditions.

Table 3: Wear volumes (x 10-3 mm^3) of pure titanium in 1xPBS, with or without BSA. Data represent mean values of n=3 measurements ± standard error.

E ($V_{Ag/Ag/Cl}$)	Solution	V_{wac}	V_{mech}	V_{tot}
-1.2 V	1xPBS	-	-	138
	1 mg/mL BSA	-	-	142
OCP	1xPBS	-	-	179
	1 mg/mL BSA	-	-	216
+1.0 V	1xPBS	23	296	319
	1 mg/mL BSA	31	535	566

316 Figure 5 shows the cross-sectional profiles of the wear track on titanium substrate acquired
317 under the same mechanical contact, as a function of surface potential (-1.2 $V_{Ag/AgCl}$, OCP, and
318 +1.0 $V_{Ag/AgCl}$), in PBS solution with or without the presence of BSA (dark and grey curves
319 respectively). The width of the generated wear track is approximately the same under all of the
320 conditions, showing accumulation of debris over the edges. The height of an undamaged circular
321 segment corresponding to a 3 mm radius sphere with an arc of 1100 µm is calculated as
322 approximately 50 µm, which is validate for anodic conditions, as shown in Figure 5c. However,
323 the height of the circular segment under cathodic conditions is substantially reduced to
324 approximately 10 µm. The maximum material loss was observed with anodic potential, while the
325 least with cathodic potential.

326 The distinctive contract between the height of the wear tracks under anodic and cathodic
327 conditions imply that a good fraction of the removed material has been smeared back onto the
328 titanium surface under cathodic conditions. It is expected that the plastic deformation at cathodic
329 conditions hardens the metal (strain hardening), which is confirmed by microindentation
330 measurements in section 3.3. For OCP and anodic potential, the presence of BSA could enhance
331 the material loss and result in deeper wear tracks, which are attributed to the increased mechanical
332 wear. Furthermore, the profiles revealed larger ridges when the BSA was present, which suggests
333 accumulation of material at the sliding interface.

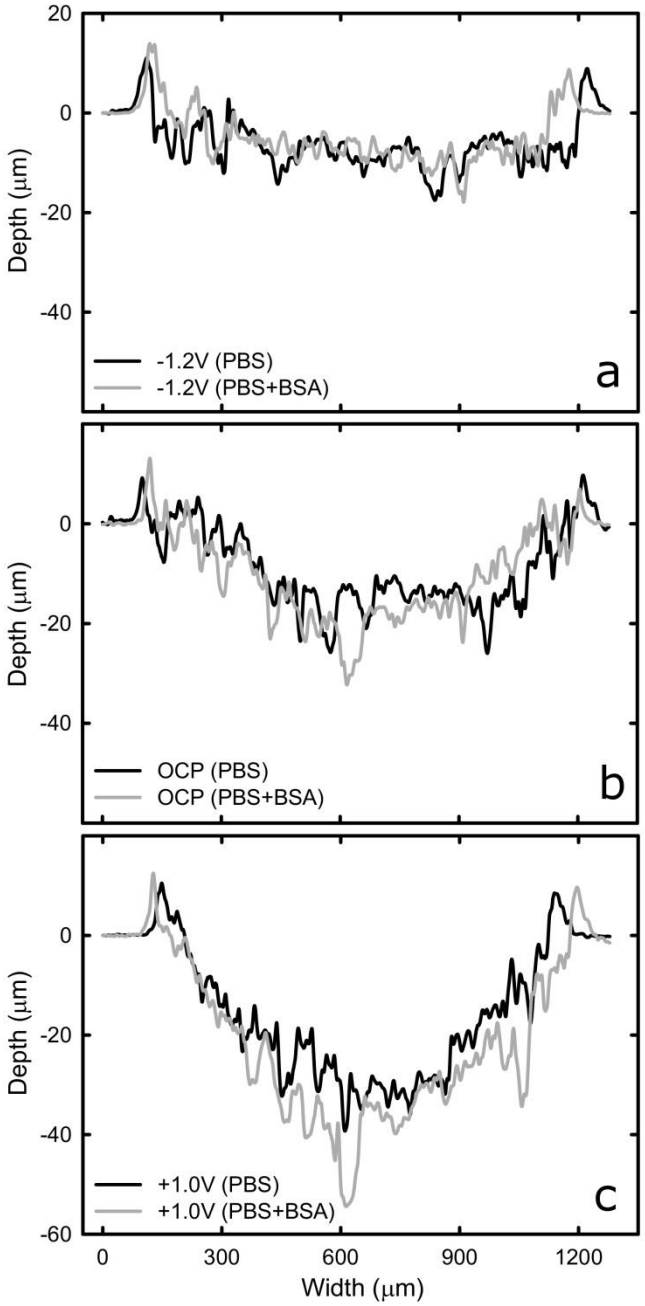

Figure 5: Wear track profile of the titanium disk under various conditions in PBS and PBS containing BSA solutions a) at cathodic applied potential, b) at open circuit potential, c) at anodic applied potential.

The profile of the wear track under cathodic conditions is less curved, while it reveals a curvature under OCP and anodic conditions. This is reflected by the wear pattern on the alumina counterparts at the end of the tribocorrosion experiments, as shown in Figure 6. The observed

patterns on the alumina are due to transfer of titanium debris on the alumina surface.[35, 36] Furthermore, a larger pattern on the alumina is observed under cathodic conditions as compared to OCP or anodic conditions, which indicates a greater amount of titanium transferred onto the alumina.

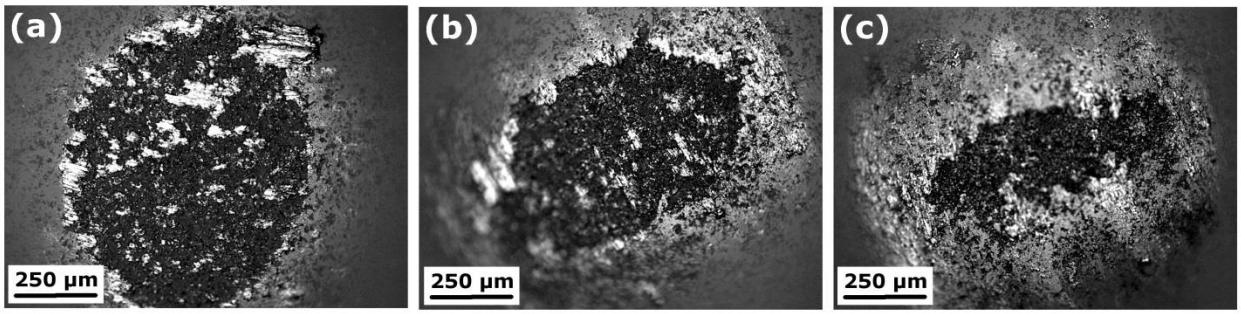

Figure 6: Optical microscopy images of alumina counterpart after the experiments in the presence of BSA at (a) -1.2 $V_{Ag/AgCl}$, (b) OCP, and (c) +1.0 $V_{Ag/AgCl}$.

The morphology of the area inside the wear tracks was acquired by SEM, as presented in Figure 7. Severe plastic deformation with signs of delamination can be observed, simultaneously to some scratches probably caused by the detached wear particles.[37]

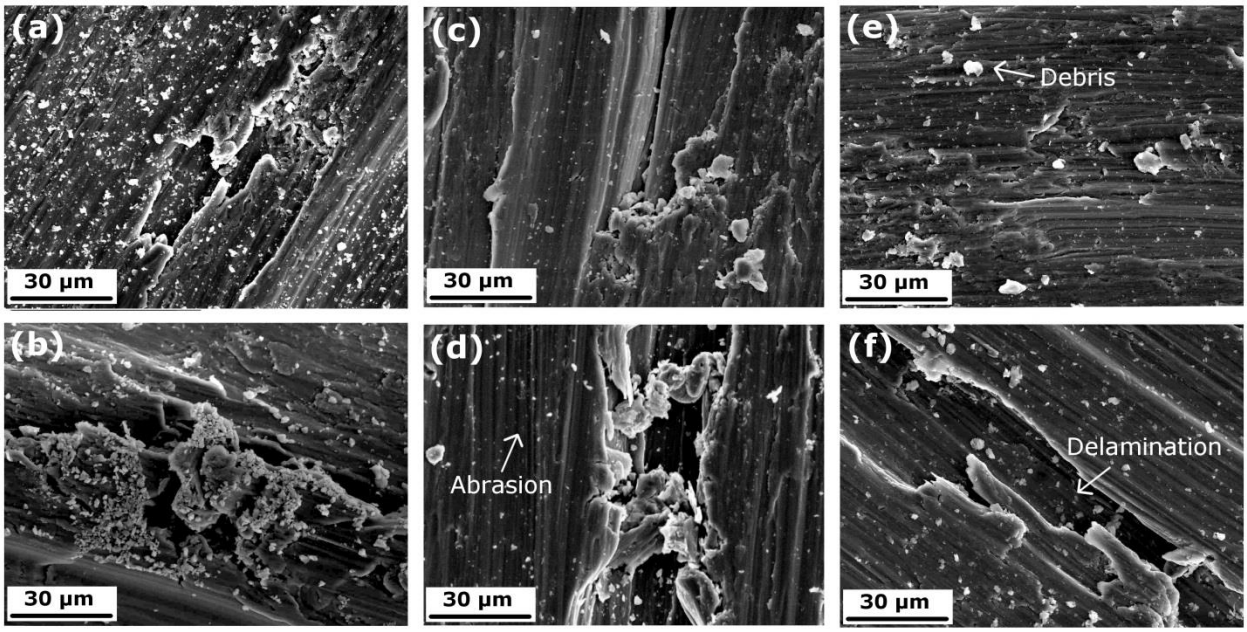

Figure 7: Scanning electron microscope images showing the topography of the wear track at (a) 1xPBS at -1.2 $V_{Ag/AgCl}$, (b) 1 mg/mL BSA in 1xPBS at -1.2 $V_{Ag/AgCl}$, (c) 1xPBS at OCP, (d) 1 mg/mL BSA in 1xPBS at OCP, (e) 1xPBS at +1.0 $V_{Ag/AgCl}$, and (f) 1 mg/mL BSA in 1xPBS at +1.0 $V_{Ag/AgCl}$.

In some cases, the debris generated as the result of surface degradation was found to aggregate and form large third bodies, with a representative one shown in Figure 8. Such large particulates present at a sliding interface could act as third body abrasives and accelerate the rate of material loss, especially in the presence of BSA due to its capacity to mediate and increase the interaction between first and third bodies and, thus, enhancing particle entrainment.[20] Most importantly, the chance of forming large debris aggregates is greater in high anodic potential than it is in low anodic potential.[38]

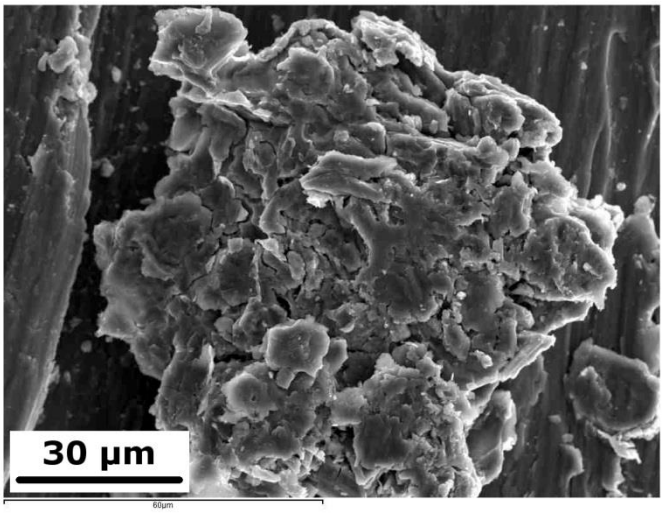

Figure 8: Scanning electron microscope image of aggregated debris inside the wear track at -1.2V in PBS containing BSA solution.

3.3 Hardness

To further understand the cause of surface degradation, a microindenter was deployed to measure the hardness within and outside of the wear track, with Figure 9 showing the hardness of

371 the titanium inside the wear track. The hardness outside the wear track is found to be equal to 120
372 HV. At cathodic and open circuit potential conditions, the hardness inside the wear track was found
373 to be approximately 250 HV showing a twofold increase compared to the hardness outside the
374 wear track, which is attributed to plastic deformation due to dislocation of atoms, in a process
375 called strain hardening.[39] At anodic applied potential conditions the increase in the hardness was
376 smaller and approximately 220 HV. The effect of BSA on hardness is not clear.

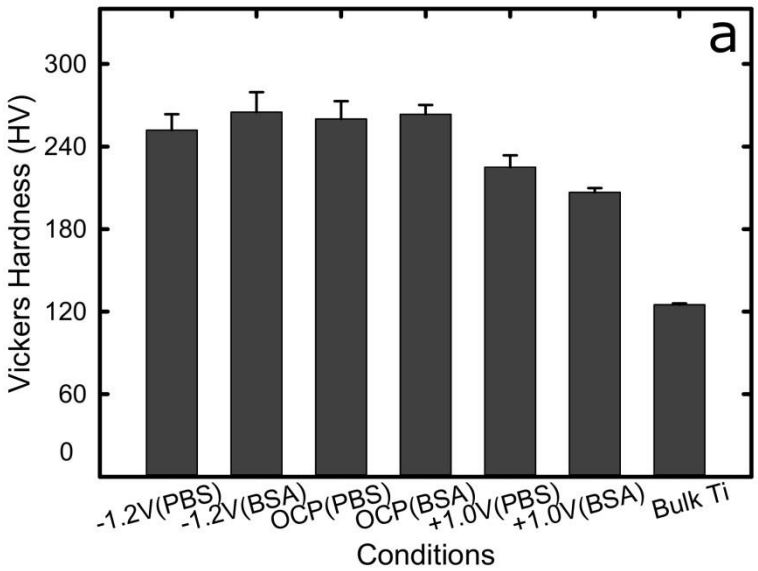

377

378 Figure 9: Hardness (Vickers) of the titanium inside and outside (bulk Ti) the wear track at various conditions. Data
379 points represent mean values of n=4 measurements ± standard error. The difference from the presence of protein is
380 insignificant (P>0.05) at -1.2 V and OCP, while it is significant (P<0.05) at +1.0 V.

381

382 **3.4 Nanoadhesion**

383 Atomic force microscopy based force measurements were carried out to quantify the adhesive
384 interaction between alumina particle and titanium surface, in the presence of BSA, under the same
385 electrochemical conditions that were used in tribocorrosion experiments. Figure 10a shows
386 representative force-distance (FD) curves collected under three different surface potentials when
387 an alumina particle was brought towards the titanium substrate, made the contact, and then

separated. For clarify purpose, only the data recorded during the separation process is shown. In the retraction curve, there are multiple peaks, so called pulling events, corresponding to the desorption of proteins. The nanoadhesion measurements offer a unique approach to quantify the interaction between alumina particle, replicating the debris generated at a sliding interface, and the solid substrate. The adhesion between alumina and titanium in PBS solution is very small (< 20 pN) and not detectable with the present cantilevers, and hence are not shown. With the presence of BSA, the adhesion force corresponds to the largest peak in the retraction curve. Throughout the nanoadhesion measurements, a number of cantilevers with alumina particle fixed at the end were used. Because variation in the size of those particles determines the contact area, all adhesion forces acquired by each cantilever were normalised against the one acquired at -1.2 $V_{Ag/AgCl}$.

Averaged values of the normalised adhesion between alumina particles against titanium in the presence of BSA under each electrochemical condition are presented in Figure 10b. The maximum adhesion was observed at cathodic potential, followed by OCP, and anodic potential where it exhibited the smallest interaction. Because the interaction between alumina and titanium in PBS was measured to be negligible, the adhesion measured here corresponds to the force needed to separate BSA molecules from alumina and titanium surfaces. Furthermore, since the interaction between alumina and BSA is expected to be the same under all electrochemical conditions studied here, the observed variation in adhesion is due to the interaction between BSA and titanium. Therefore, the presence of BSA increases the adhesion of the debris at the interface between the sliding surfaces. Under anodic conditions, the adhesion is slightly lower than cathodic ones.

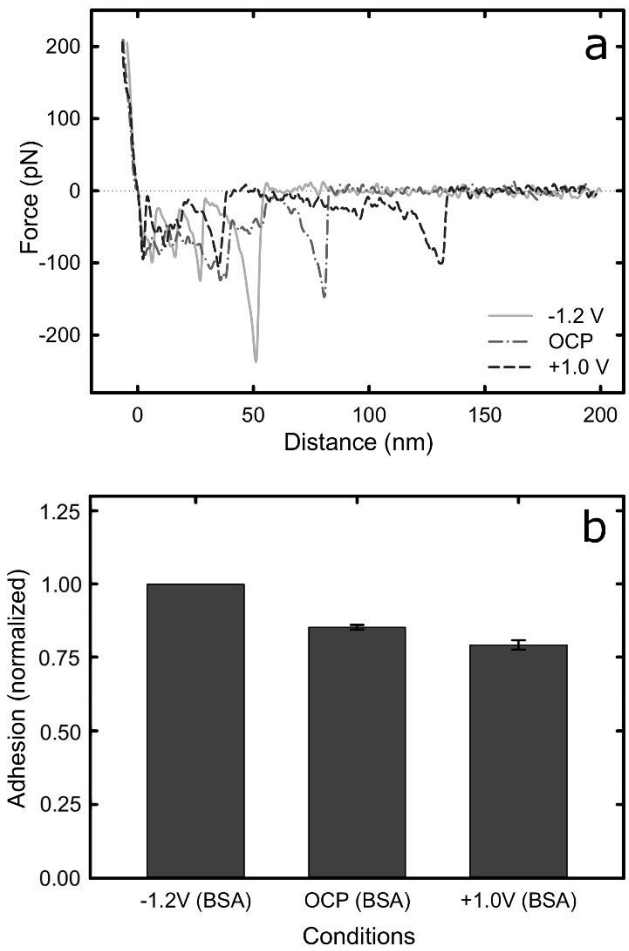

Figure 10: (a) Representatives force-distance curves of alumina against titanium, and (b) adhesion between alumina and titanium surface, in the presence of BSA at -1.2 $V_{Ag/AgCl}$, OCP, and +1.0 $V_{Ag/AgCl}$. Adhesion in the absence of BSA was negligible and not shown. Data points represent mean values of n=600 measurements ± standard error ($P<0.05$).

4 Discussion

4.1 Effect of electrode potential on the tribocorrosion damage of titanium

The passive film formed on the titanium surface is highly depended on the prevailing electrochemical conditions. Under the selected cathodic applied potential, titanium surface remains passive[40] and reduction reactions (mainly water and oxygen) would take place on the surface. However, anodic oxidation of titanium could be more favoured, resulting in thicker oxide

421 films when anodic potential is applied. Therefore, it is sensible to assume that an oxide film is
422 present on the titanium surface when being exposed to electrolyte under all electrochemical
423 conditions in the present study. Furthermore, previous study suggested that reduction of titanium
424 oxide is a hard to achieve.[41] Upon initiation of sliding, the passive film is mechanically detached
425 from the surface, leaving the active titanium underneath exposed and causing the OCP to drop and
426 the current to increase. Without the passive film to protect the surface, the corrosion rate is greatly
427 increased. When the sliding stops, the passive film is quickly regenerated on the titanium surface
428 and protects from further corrosion.
429
430 During tribocorrosion, two wear mechanisms are present; wear accelerated corrosion that
431 occurs with the elimination of the passive film by mechanical disruption and repassivation of the
432 surface, and mechanical wear by plastic deformation.[15] The total material loss is significantly
433 increased at anodic conditions as oppose to cathodic or OCP. Although the corrosion is greatly
434 increased upon removal of the passive film at anodic conditions, the contribution of the corrosion
435 to the total mass loss is only 7%, with the rest due to mechanical wear. Therefore, the increased
436 material loss is due to the effect of the presence of a thicker passive film on the mechanical
437 behaviour of the material.[15] It is believed (and in good agreement with the nano-adhesion
438 measurements which show higher adhesive forces at an applied cathodic potential) that the
439 detached metallic particles are easily deformed and smeared back on the wear track area at cathodic
440 potential, which in turn reduces the rate of wear loss. As a result of the increased plastic
441 deformation and smearing at cathodic conditions, the hardness of titanium is increased due to strain
442 hardening, as suggested by the results in Figure 9.

The increased mechanical wear at anodic conditions could also be attributed to an increased presence of debris at the sliding interface. This is in agreement with a previous study where it was found that the formed debris metallic particles were dissolved in the electrolyte at low anodic potential before they could form a large third body.[38] In contrast, at higher anodic current, the formed metallic debris have sufficient time to repassivate and form large wear debris (Figure 8). The newly formed third bodies are in turn act as abrasive particles during sliding that accelerates the mechanical material removal.

4.2 Effect of albumin on tribocorrosion characteristics of titanium

It has been found that albumin could act as a cathodic inhibitor in PBS solution - it reduces the rate of cathodic reactions, which in turn shifts the corrosion potential and the cathodic current towards more cathodic values.[17] This is consistent with the present work, as shown in Figure 1 and Figure 2a, where the reduction in the cathodic reactions rates shifted the OCP towards lower values and decreases the cathodic current under cathodic polarization condition in the presence of BSA. It was also suggested that the adsorbed BSA molecules on the titanium surface could hinder the transport of oxygen towards the solid/liquid interface and, consequently, inhibit the rate of oxygen reduction.[17, 42, 43] At the same time, protein molecules could bound metal ions and carry them away from the solid/liquid interface, which in turn accelerates the rate of anodic reactions.[44, 45] This second mechanism is apparent in Figure 2b where the presence of BSA results in a current increase.

The presence of albumin in the PBS solutions increases significantly the mechanical wear (Figure 4), which is attributed to two factors as was shown by the force-distance curves (Figure 10). Firstly, BSA increases the adhesion of debris onto the sliding surfaces, causing an increased amount of debris present at the sliding interface and, thus, greater mechanical wear. This is

467 suggested by the nanoadhesion measurements between alumina and titanium - the adhesion is
468 negligible in PBS but increases greatly in the presence of BSA. Secondly, the presence of albumin
469 under anodic conditions further increases the mechanical wear, which is likely due to a
470 combination of an increased presence of debris and a reduction in the adhesion between BSA and
471 titanium particles at anodic potential (Figure 10b). This is consistent with previous study where it
472 was found that protein enhances the efficiency of the abrasives (third bodies) and leads to larger
473 material loss.[20]
474

475 **5 Conclusions**

476 In the present study, the tribocorrosion behaviour of pure titanium and the effect of BSA on it
477 have been studied. For that, different electrochemical conditions (i.e. cathodic and anodic
478 potentials) were applied at the titanium surfaces and in all cases a passive layer with different
479 thicknesses was found to form on the surface. Upon mechanical damage, the active titanium
480 underneath is being exposed and the corresponding corrosion rate is significantly increased. The
481 total material loss during tribocorrosion of titanium is highly attributed to the mechanical wear,
482 while the wear accelerated corrosion is only a small fraction of the total loss. The mechanical wear
483 is caused by plastic deformation and detachment of particles, while it is further increased at anodic
484 conditions due to greater presence of debris particles at the sliding interface.
485

486 The presence of BSA inhibits the repassivation rate of oxide film by hindering the rate of
487 cathodic reaction, while it also accelerates the rate of anodic reactions. Albumin was also found to
488 significantly increase the mechanical wear by increasing the adhesion of the debris on the sliding
489 interface. Furthermore, an increased mechanical wear was observed at anodic conditions, which

could be attributed to a combination of an increased presence of titanium third bodies and reduced adhesion with protein that could enhance their wear efficiency.

Acknowledgments

ZJZ acknowledges financial support from the Engineering and Physical Science Research Council (EPSRC) under project EP/P007864/1 and the Royal Society (IE161008).

References

1. Roach M. Base metal alloys used for dental restorations and implants. *Dent Clin North Am* 2007, **51**(3)**:** 603-627, vi.

2. Nosonovsky M, Bhushan B. Green tribology: principles, research areas and challenges. *Philos Trans A Math Phys Eng Sci* 2010, **368**(1929)**:** 4677-4694.

3. Niinomi M. Mechanical properties of biomedical titanium alloys. *Materials Science and Engineering a-Structural Materials Properties Microstructure and Processing* 1998, **243**(1-2)**:** 231-236.

4. Koike M, Fujii H. The corrosion resistance of pure titanium in organic acids. *Biomaterials* 2001, **22**(21)**:** 2931-2936.

5. Niinomi M. Biologically and mechanically biocompatible titanium alloys. *Materials Transactions* 2008, **49**(10)**:** 2170-2178.

6. Hanawa T. Metal ion release from metal implants. *Materials Science & Engineering C-Biomimetic and Supramolecular Systems* 2004, **24**(6-8)**:** 745-752.

7. Elias CN, Lima JHC, Valiev R, Meyers MA. Biomedical applications of titanium and its alloys. *JOM* 2008, **60**(3)**:** 46-49.

8. Tathe A, Ghodke M, Nikalje AP. A brief review: biomaterials and their application. *International Journal of Pharmacy and Pharmaceutical Sciences* 2010, **2**(4)**:** 19-23.

523 9. Prasad S, Ehrensberger M, Gibson MP, Kim H, Monaco EA. Biomaterial properties of titaniumin
524 dentistry. *J Oral Biosci* 2015, **57**(4)**:** 192-199.

525
526 10. Rack HJ, Qazi JI. Titanium alloys for biomedical applications. *Materials Science & Engineering C-*
527 *Biomimetic and Supramolecular Systems* 2006, **26**(8)**:** 1269-1277.

528
529 11. Manam NS, Harun WSW, Shri DNA, Ghani SAC, Kurniawan T, Ismail MH*, et al.* Study of corrosion
530 in biocompatible metals for implants: A review. *J Alloys Compd* 2017, **701:** 698-715.

531
532 12. Landolt D, Mischler S. *Tribocorrosion of passive metals and coatings*. Woodhead: Oxford ;
533 Philadelphia, 2011.

534
535 13. Maldonado SG, Mischler S, Cantoni M, Chitty WJ, Falcand C, Hertz D. Mechanical and chemical
536 mechanisms in the tribocorrosion of a Stellite type alloy. *Wear* 2013, **308**(1-2)**:** 213-221.

537
538 14. Rituerto Sin J, Neville A, Emami N. Corrosion and tribocorrosion of hafnium in simulated body
539 fluids. *J Biomed Mater Res B Appl Biomater* 2014, **102**(6)**:** 1157-1164.

540
541 15. Mischler S, Spiegel A, Landolt D. The role of passive oxide films on the degradation of steel in
542 tribocorrosion systems. *Wear* 1999, **225:** 1078-1087.

543
544 16. Foghandersen N, Altura BM, Altura BT, Siggaardandersen O. Composition of interstitial fluid. *Clin*
545 *Chem* 1995, **41**(10)**:** 1522-1525.

546
547 17. Hiromoto S, Mischler S. The influence of proteins on the fretting-corrosion behaviour of a Ti6Al4V
548 alloy. *Wear* 2006, **261**(9)**:** 1002-1011.

549
550 18. Khan MA, Williams RL, Williams DF. Conjoint corrosion and wear in titanium alloys. *Biomaterials*
551 1999, **20**(8)**:** 765-772.

552
553 19. Hanawa T, Kohayama Y, Hiromoto S, Yamamoto A. Effects of biological factors on the
554 repassivation current of titanium. *Materials Transactions* 2004, **45**(5)**:** 1635-1639.

555
556 20. Sun D, Wharton JA, Wood RJK. Effects of proteins and pH on tribocorrosion performance of cast
557 CoCrMo – a combined electrochemical and tribological study. *Tribology - Materials, Surfaces &*
558 *Interfaces* 2013, **2**(3)**:** 150-160.

559
560 21. Munro RG. Evaluated material properties for a sintered alpha-alumina. *J Am Ceram Soc* 1997,
561 **80**(8)**:** 1919-1928.

562
563 22. Adams GG, Nosonovsky M. Contact modeling forces. *Tribology International* 2000, **33**(5-6)**:** 431-
564 442.

565
566 23. Hutter JL, Bechhoefer J. Calibration of atomic force microscope tips. *Rev Sci Instrum* 1993, **64**(7)**:**
567 1868-1873.

568
569 24. Liamas E, Mulheran PA, Black RA, Thomas ORT, Munoz AI, Zhang ZJ. Electrochemical behaviour of
570 titanium in protein-containing saline solution. *RSC Adv*. 2019 Accepted.

571
572 25. Munoz AI, Mischler S. Electrochemical quartz crystal microbalance and x-ray photoelectron
573 spectroscopy study of cathodic reactions in bovine serum albumin containing solutions on a
574 physical vapour deposition CoCrMo biomedical alloy. *Electrochim Acta* 2015, **180:** 96-103.

575
576 26. Pourbaix M. *Atlas of electrochemical equilibria in aqueous solutions*, 2d English edn. National
577 Association of Corrosion Engineers: Houston, Tex., 1974.

578
579 27. Milosev I, Zerjav G, Moreno JMC, Popa M. Electrochemical properties, chemical composition and
580 thickness of passive film formed on novel Ti-20Nb-10Zr-5Ta alloy. *Electrochim Acta* 2013, **99:** 176-
581 189.

582
583 28. Olsson COA, Verge MG, Landolt D. EQCM study of anodic film growth on valve metals. *J*
584 *Electrochem Soc* 2004, **151**(12)**:** B652-B660.

585
586 29. Milosev I, Metikos-Hukovic M, Strehblow HH. Passive film on orthopaedic TiAlV alloy formed in
587 physiological solution investigated by X-ray photoelectron spectroscopy. *Biomaterials* 2000,
588 **21**(20)**:** 2103-2113.

589
590 30. Verge MG, Mettraux P, Olsson COA, Landolt D. Rotating ring-disk electrochemical quartz crystal
591 microbalance: a new tool for in situ studies of oxide film formation. *J Electroanal Chem* 2004,
592 **566**(2)**:** 361-370.

593
594 31. Milosev I, Kosec T, Strehblow HH. XPS and EIS study of the passive film formed on orthopaedic Ti-
595 6Al-7Nb alloy in Hank's physiological solution. *Electrochim Acta* 2008, **53**(9)**:** 3547-3558.

596
597 32. Licausi MP, Munoz AI, Borras VA. Tribocorrosion mechanisms of Ti6Al4V biomedical alloys in
598 artificial saliva with different pHs. *Journal of Physics D-Applied Physics* 2013, **46**(40).

599
600 33. Bazzoni A, Mischler S, Espallargas N. Tribocorrosion of pulsed plasma nitrided CoCrMo implant
601 alloy. *Tribol Lett* 2013, **49**(1)**:** 157-167.

602
603 34. Mischler S. Triboelectrochemical techniques and interpretation methods in tribocorrosion: A
604 comparative evaluation. *Tribology International* 2008, **41**(7)**:** 573-583.

605
606 35. Munoz AI, Mischler S. Effect of the environment on wear ranking and corrosion of biomedical
607 CoCrMo alloys. *J Mater Sci Mater Med* 2011, **22**(3)**:** 437-450.

608
609 36. Pina VG, Dalmau A, Devesa F, Amigo V, Munoz AI. Tribocorrosion behavior of beta titanium
610 biomedical alloys in phosphate buffer saline solution. *J Mech Behav Biomed Mater* 2015, **46:** 59-
611 68.

612
613 37. Molinari A, Straffelini G, Tesi B, Bacci T. Dry sliding wear mechanisms of the Ti6Al4V alloy. *Wear*
614 1997, **208**(1-2)**:** 105-112.

615
616 38. Landolt D, Mischler S, Stemp M, Barril S. Third body effects and material fluxes in tribocorrosion
617 systems involving a sliding contact. *Wear* 2004, **256**(5)**:** 517-524.

618
619 39. Askeland RD. *The science and engineering of materials*, Si edition. edn. Cengage Learning: Mason,
620 OH, 2015.

621
622 40. Contu F. The cathodic behavior of titanium: Serum effect. *J Biomed Mater Res B Appl Biomater*
623 2012, **100**(2)**:** 544-552.

624
625 41. Chen GZ, Fray DJ, Farthing TW. Direct electrochemical reduction of titanium dioxide to titanium
626 in molten calcium chloride. *Nature* 2000, **407**(6802)**:** 361-364.

627
628 42. Vidal CV, Munoz AI. Electrochemical characterisation of biomedical alloys for surgical implants in
629 simulated body fluids. *Corros Sci* 2008, **50**(7)**:** 1954-1961.

630
631 43. Munoz AI, Mischler S. Interactive effects of albumin and phosphate ions on the corrosion of
632 CoCrMo implant alloy. *J Electrochem Soc* 2007, **154**(10)**:** C562-C570.

633
634 44. Khan MA, Williams RL, Williams DF. The corrosion behaviour of Ti-6Al-4V, Ti-6Al-7Nb and Ti-13Nb-
635 13Zr in protein solutions. *Biomaterials* 1999, **20**(7)**:** 631-637.

636
637 45. Lewis AC, Kilburn MR, Heard PJ, Scott TB, Hallam KR, Allen GC*, et al.* The entrapment of corrosion
638 products from CoCr implant alloys in the deposits of calcium phosphate: a comparison of serum,
639 synovial fluid, albumin, EDTA, and water. *J Orthop Res* 2006, **24**(8)**:** 1587-1596.

640

641